

$\sin^2\theta_W$ estimate and bounds on nonstandard interactions at source and detector in the solar neutrino low-energy regime

Amir N. Khan*

School of Physics, Sun Yat-Sen University, Guangzhou, Guangdong, 510275, P. R. China

Douglas W. McKay†

Department of Physics and Astronomy, University of Kansas, Lawrence, KS 66045, USA

(Dated: August 2, 2017)

We explore the implications of the Borexino experiment's real time measurements of the lowest energy part of the neutrino spectrum from the primary pp fusion process up to 0.420 MeV through the ${}^7\text{Be}$ decay at 0.862 MeV to the pep reaction at 1.44 MeV. We exploit the fact that at such low energies, the large mixing angle solution to the Mikheyev-Smirnov-Wolfenstein matter effects in the sun are small for ${}^7\text{Be}$ and pep and negligible for pp . Consequently, the neutrinos produced in the sun change their flavor almost entirely through vacuum oscillations during propagation from the sun's surface and through possible nonstandard interactions acting at the solar source and Borexino detector. We combine the different NSI effects at source and detector in a single framework and use the current Borexino data to bound NSI non-universal and flavor-changing parameters at energies below the reach of reactor neutrino experiments. We also study the implication of the current data for the weak-mixing angle at this "low-energy frontier" data from the Borexino experiment, where it is expected to be slightly larger than its value at the Z mass. We find $\sin^2\theta_W = 0.224 \pm 0.016$, the lowest energy-scale estimate to date. Looking to the future, we use projected sensitivities to solar neutrinos in next generation dedicated solar experiments and direct dark matter detection experiments and find a potential factor five improvement in determination of the weak-mixing angle and up to an order of magnitude improvement in probing the NSI parameters space.

I. INTRODUCTION

Experimental and theoretical studies of solar neutrinos have played a special role in our understanding of solar structure and dynamics [1] and the interaction and propagation of neutrinos themselves [2]. Reviews of the current picture and some prospects for the future can be found in Refs. [3–5]. Here we focus on the lowest energy range of solar neutrinos, whose sources are the pp , ${}^7\text{Be}$ and pep processes. In recent years, the Borexino experiment [6–9] has published for the first time the discovery or strong evidence for direct detection of all three of these neutrino sources, providing neutrino detection rates that can probe the predictions of the value of the weak-mixing angle at and below an MeV and the possibility of deviations from the predictions of the standard model (SM) in the form of nonstandard interactions (NSIs).

Neutrinos produced at the Sun are detected at the Borexino detector using the purely leptonic elastic processes $e+\nu \rightarrow e+\nu$ at neutrino energies roughly in the range $0.3m_e \leq E_\nu \leq 3m_e$ [6–8]. In this region, the energy dependence of the large mixing angle Mikheyev-Smirnov-Wolfenstein [10–12] (LMA-MSW) mixing is weak, and we take the NSI effects to be concentrated in the source and detector, where we focus our attention in this work.¹ The structure of the problem is quite similar to the problem of NSI effects in very short-baseline reactor neutrino data, with the key difference that the energy-independent, oscillation length-averaged solar propagation factor brings in mixing parameters and carries source terms that are *linear* in the flavor-changing (FC) NSI parameters. This gives an advantage in sensitivity over the very short-baseline case, where these NSIs appear only quadratically.

In our formalism, described in Sec. 2, we combine source NSIs with detector NSIs in a unified framework. To a first approximation, excellent in the pp case, the oscillation probabilities in the low-energy region are energy-independent, the result of averaging over the long propagation distances. Since the source NSIs are included in the oscillation probabilities, there is little energy dependence involving the NSI parameters. On the other hand, the

*Electronic address: ntrnphysics@gmail.com, khan8@mail.sysu.edu.cn

†Electronic address: dmckay@ku.edu

¹ Typically, works on solar NSI effects [13–16], have included the whole solar spectrum and have taken the opposite point of view, making detailed studies of the propagation effects and not including the direct source and detector NSI contributions. For the completely opposite view, where a solution of the solar neutrino problem was sought using *only* NSI, in the spirit of [11], see [17].

detector ν -e cross sections depend strongly on neutrino energy, including energy dependence due to the NSIs at the detector. As a result, the convolution of the flux, the oscillation probabilities and the cross sections over the neutrino energy spectrum introduces energy dependence in the rate that is almost entirely due to the detector. The resulting event rate treatment is outlined in Sec. 3. To approximate the small P_{ee} variation with energy expected from the standard mixing model (SMM) and LMA-MSW model as E_ν rises to the ${}^7\text{Be}$ and pep sources, we evaluate the count rates with the electron survival probability reduced by the appropriate factors relative to pp . As our first application, we turn off the NSIs and fit $\sin^2(\theta_W)$ to the Borexino low-energy data in Sec. 4 and compare to the results of several other studies [18–20].

In our study of reactor short-baseline experiments [18, 19], we showed that the data can not provide absolute bounds on the FC leptonic NSI parameters involving $\bar{\nu}_\mu$ or $\bar{\nu}_\tau$, because as the relevant *source* NSI parameters approach zero, it leaves only incident $\bar{\nu}_e$ s, which cannot oscillate appreciably to $\bar{\nu}_\mu$ or $\bar{\nu}_\tau$ in the 10s of meters baselines like TEXONO [21], LSND [22] or KARMEN [23]. This is not true in the present study, where the solar ν_e s oscillate significantly to ν_μ s and ν_τ s, providing “wrong flavor” neutrinos at the detector and subsequent bounds on the FC leptonic NSI parameters even when the source FC NSIs are turned off. Because the oscillation and flavor-changing NSI produce similar and sometimes mutually supporting effects, the interesting problem of disentangling them arises. Those NSI processes that do not involve oscillations such as those in very short-baseline neutrino scattering and nuclear and particle decay experiments then play an important role. We expand on this question upon closing in Sec. VII.

The solar low-energy neutrino spectrum study is potentially ideal for the study of NSI phases. As we noted in Refs. [18, 19], reactor data shows more sensitivity to these phases at the very low-energy end of the neutrino spectrum. This is because the energy-dependent coefficients of the phase-dependent terms, which are proportional to the electron mass m_e , becomes comparable to that of the other terms as the neutrino energy becomes of the order of m_e or less. This makes the pp -chain neutrino region below 1 MeV valuable for the NSI phase information. The present work can be viewed as complementary to analyses of the TEXONO reactor experiment [21, 24], for example. Both experiments involve a semi-leptonic process at the source and detection of a recoil electron from an elastic neutrino-electron scattering at the detector. In the solar case, ν_e s are the beam neutrinos, while in the reactor case $\bar{\nu}_e$ s are the incident beam, and, as already noted, the solar analysis requires oscillations while the reactor analysis does not. We fit the source NSIs with solar data in Sec. 5, the detector NSIs in Sec. 6.

As noted in Ref. [6] if the Borexino precision is extended to reach the 1% level, it gives powerful leverage to determine the solar metallicity and to explore neutrino properties. As dark-matter experiments reach levels of sensitivity where solar background events become a problem, in effect they become sensitive solar neutrino detectors [25–28] that can combine with future high sensitivity multi-purpose neutrino experiments [29–34] to make orders of magnitude increases in the quality of low-energy solar physics data. We estimate the sensitivity to NSI parameters that would be possible with these developments in Sec. 7, commenting on the level of tightening of bounds on NSIs compared to those following from the current data. In addition, we analyze source and detector cross correlations among our future prospects possibilities and describe the origins of several of the striking correlations that we find. We summarize and conclude in Sec. 8. Our treatment of the pp neutrino flux is given in an Appendix.

II. FORMALISM AND NOTATION

In this section we review all of the essential neutrino effective Lagrangian, neutrino mixing and neutrino oscillation formulas in the presence of non-universal (NU) and FC neutrino interactions, defining relevant notation as we go.

A. NSI effective Lagrangians at source and detector

For the general setup under consideration, the sources of neutrinos and antineutrinos are the nuclear fusion/decay processes in the sun, nuclear beta decays in reactor cores or the pion decays at accelerators, while the target particles at the detectors are electrons. Therefore the effective four-Fermi Lagrangians governing the charged-current (CC) semi-leptonic processes at the source [18, 19, 35–39] and the (anti)neutrinos-electron scattering processes [18, 19] at the detector are given as

$$\mathcal{L}^s = \mathcal{L}_{NU}^s + \mathcal{L}_{FC}^s \quad (1)$$

$$\mathcal{L}^\ell = \mathcal{L}_{NU}^\ell + \mathcal{L}_{FC}^\ell \quad (2)$$

where,

$$\mathcal{L}_{NU}^s = -2\sqrt{2}G_F \sum_{a,\alpha} (1 + \varepsilon_{\alpha\alpha}^{udL}) (\bar{l}_\alpha \gamma_\lambda P_L U_{\alpha a} \nu_a) (\bar{d} \gamma^\lambda P_L u)^\dagger + h.c., \quad (3)$$

$$\mathcal{L}_{FC}^s = -2\sqrt{2}G_F \sum_{a,\alpha \neq \beta} \varepsilon_{\alpha\beta}^{udL} (\bar{l}_\alpha \gamma_\lambda P_L U_{\beta a} \nu_a) (\bar{d} \gamma^\lambda P_L u)^\dagger + h.c., \quad (4)$$

$$\mathcal{L}_{NU}^\ell = -2\sqrt{2}G_F \sum_{\alpha} (\bar{e} \gamma_\lambda (\tilde{g}_{\alpha R} P_R + (\tilde{g}_{\alpha L} + 1) P_L) e) (\bar{\nu}_\alpha \gamma^\lambda P_L \nu_\alpha), \quad (5)$$

$$\mathcal{L}_{FC}^\ell = -2\sqrt{2}G_F \sum_{\alpha \neq \beta} \varepsilon_{\alpha\beta}^{eP} (\bar{e} \gamma_\lambda P e) (\bar{\nu}_\alpha \gamma^\lambda P_L \nu_\beta). \quad (6)$$

Here the superscript s and ℓ designate semi-leptonic and purely leptonic Lagrangians and the subscripts NU and FC correspond to the NU and FC NSIs for both cases. α and β are the flavor-basis indices and a is mass-basis index². The complex coefficients $\varepsilon_{\alpha\beta}^{udL}$ represent the relative coupling strengths of the flavor combinations in the presence of new physics at solar, accelerator or reactor sources and the complex coefficients $\varepsilon_{\alpha\beta}^{eP}$ represent the relative coupling strengths of the flavor combinations in the presence of new physics at the detector, while in the SM $\varepsilon_{\alpha\beta}^{udL} = 0$ and $\varepsilon_{\alpha\beta}^{eP} = 0$. The NU , flavor-diagonal interactions contain the NSI parameters $\varepsilon_{\alpha\alpha}^{udL}$ at the source and both $\varepsilon_{\alpha\alpha}^{eR}$ and $\varepsilon_{\alpha\alpha}^{eL}$ at the detector, where these are implicitly given in the definitions of the coefficients $\tilde{g}_{\alpha R}$ and $\tilde{g}_{\alpha L}$, where $\tilde{g}_{\alpha R} = \sin^2 \theta_W + \varepsilon_{\alpha\alpha}^{eR}$ and $\tilde{g}_{\alpha L} = \sin^2 \theta_W - \frac{1}{2} + \varepsilon_{\alpha\alpha}^{eL}$. The hermiticity of the pure leptonic effective Lagrangian, \mathcal{L}^ℓ , requires that the detector NSI parameter matrix is Hermitian and therefore, $\varepsilon_{\alpha\beta}^{eR,L} = (\varepsilon_{\beta\alpha}^{eR,L})^*$, so the NU NSI parameters are real, but the FC NSI parameters are complex in general. With the effective Lagrangians defined, we turn next to the cross sections and flux factors needed for the study of the NSI effects at the source and detector.

B. Neutrino oscillation probabilities at Earth

For neutrinos at the low-energy end of the solar spectrum from pp ,⁷ Be and pep reactions, the LMA-MSW expectation is that the mixing at Earth is essentially the vacuum oscillation result. For example, Ref. [40] makes this assumption and uses the Borexino 7Be data to bound leptonic NSI parameters that enter the flavor-diagonal elastic ν -e cross section at the detector. We review the SMM case and the NSI contributions in this section, returning to the small, low-energy LMA-MSW effects in the following section.

1. The standard mixing model result

The oscillation amplitude takes the matrix form $A_{\alpha\beta} = U_{\alpha a} X_a U_{a\beta}^\dagger$, where the flavor labels are Greek letters, α and β in this case (summation over repeated indices is implied). One can include NSIs in matrix form, such as $(1 + \varepsilon^{udL})U$ and the following argument still applies, because the averaging involves only the mass basis indices a, b, c, \dots . The U matrix is the neutrino mixing matrix for any number of neutrinos and the X is the diagonal phase matrix $X = \text{diag}(1, \exp(-i2\pi L/L_{21}^{osc}), \exp(-i2\pi L/L_{31}^{osc}), \dots)$. The oscillation length is defined as $L_{ab}^{osc} = 4\pi E / (m_a^2 - m_b^2)$. The oscillation probability can be written as

$$P_{\alpha\beta} = |A_{\alpha\beta}|^2 = |U_{\alpha a} X_a U_{a\beta}^*|^2, \quad (7)$$

so the average over an oscillation length is then

$$\langle P \rangle_{\alpha\beta} = U_{\alpha a} U_{\beta a}^* U_{\alpha a}^* U_{\beta a} = |U_{\alpha a}|^2 |U_{\beta a}|^2, \quad (8)$$

² For simplicity, we consider only the left-handed quark helicity states and do not include the right-handed terms in our discussion. The parameters $\varepsilon_{\alpha\beta}^{udL}$ are called $K_{\alpha\beta}$ in Ref. [18, 35].

for the average over one cycle of the probability function. For example, the electron survival averaged probability is $\langle P \rangle_{ee} = (c_{12}c_{13})^4 + (s_{12}c_{13})^4 + s_{13}^4$, in the most commonly used basis and notation [41], where $s_{ij} \equiv \sin \theta_{ij}$ and $c_{ij} \equiv \cos \theta_{ij}$.

C. The NSI effects at the source with oscillations

For the case where there are NSIs only at the source, which in the solar neutrino case means the semi-leptonic, or ϵ^{udL} parameters, we can write the matrix form of the amplitude A as

$$A_{\alpha\beta} = [(1 + \epsilon^{udL})UXU^\dagger]_{\alpha\beta}. \quad (9)$$

After averaging over an oscillation length to get the oscillation average probability for our application, we have

$$\begin{aligned} \langle P \rangle_{\alpha\beta}^{NSI} &= |(1 + \epsilon^{udL})U]_{\alpha a}|^2 |U_{\beta a}|^2 \\ &= (|U_{\alpha a}|^2 + 2 \operatorname{Re}(U_{\alpha a} \epsilon_{\alpha\gamma}^{udL*} U_{\gamma a}^*) + |\epsilon_{\alpha\gamma}^{udL} U_{\gamma a}|^2) |U_{\beta a}|^2. \end{aligned} \quad (10)$$

The low-energy ν survival probability³ from the solar core to Earth is then

$$\begin{aligned} \langle P \rangle_{ee}^{NSI} &= (|U_{ea}|^2 + 2 \operatorname{Re}(U_{ea} \epsilon_{ee}^{udL*} U_{ea}^* + U_{ea} \epsilon_{e\mu}^{udL*} U_{\mu a}^* + U_{ea} \epsilon_{e\tau}^{udL*} U_{\tau a}^*) \\ &\quad + |\epsilon_{ee}^{udL} U_{ea}|^2 + |\epsilon_{e\mu}^{udL} U_{\mu a}|^2 + |\epsilon_{e\tau}^{udL} U_{\tau a}|^2) |U_{ea}|^2. \end{aligned}$$

Working to linear order in the FC $\epsilon_{\alpha\beta}^{udL}$ parameters, the expression for the electron neutrino survival probability is found to be

$$\begin{aligned} \langle P \rangle_{ee}^{NSI} &= (1 + 2 \operatorname{Re} \epsilon_{ee}^{udL} + |\epsilon_{ee}^{udL}|^2) \langle P \rangle_{ee}^{SMM} - (c_{23}\epsilon_-) c_{13}^3 \sin 2\theta_{12} \cos 2\theta_{12} \\ &\quad + (c_{23}\epsilon_+) (\frac{1}{2} c_{13}^2 \sin 2\theta_{13} \sin^2 2\theta_{12} - \sin 2\theta_{13} \cos 2\theta_{13}), \end{aligned} \quad (11)$$

where $\langle P \rangle_{ee}^{SMM}$ is the average standard oscillation probability as given below Eq. (8). The parameter combinations $c_{23}\epsilon_+$ and $c_{23}\epsilon_-$ are defined as

$$\begin{aligned} c_{23}\epsilon_+ &\equiv |\epsilon_{e\mu}^{udL}| \cos(\phi_{e\mu} + \delta_{CP}) s_{23} + |\epsilon_{e\tau}^{udL}| \cos(\phi_{e\tau} + \delta_{CP}) c_{23} \\ c_{23}\epsilon_- &\equiv |\epsilon_{e\mu}^{udL}| \cos \phi_{e\mu} c_{23} - |\epsilon_{e\tau}^{udL}| \cos \phi_{e\tau} s_{23}, \end{aligned} \quad (12)$$

which are the two observable FC parameters that appear at linear order, which is why we focus on them in the present work as we did for the medium-baseline experimental set up in Ref. [35]. As Eq. (12) reminds us, when the NSI are present the CP violating phase δ of the SMM appears in P_{ee} inextricably intertwined with the the NSI CP-violating phases [35, 38, 42, 43]. We will return to this point in our discussion of the Borexino constraints on source NSI parameters in Sec. V.

The coefficients of the NSI in all of the above equations involve the oscillation mixing angles, which leads in some applications to ambiguities between the roles of the two parameter sets [35, 36]. This is especially clear in the linear, FC terms in Eq. 11. In our numerical work we will set the mixing parameters to their central values in the 2016 Particle Data Group review [41]. We return to this point in Sec. VII, where we describe several ways that degeneracies can be constrained and give an example.

³ When flavor-violating NSI are active, $\langle P \rangle_{ee}^{NSI}$ means the probability that a neutrino produced with a positron at the source arrives as a ν_e to produce a recoiled electron at the detector.

D. NSI effects at the solar neutrino detector

The Lagrangian given in Eq. (2), leads to the following total cross sections for the $\nu_e e-$ and $\nu_{\mu,\tau} e-$ scattering cases, similar to those calculated in Ref. [18], for $\bar{\nu}_e e-$ and $\bar{\nu}_{\mu,\tau} e-$ scattering,

$$\begin{aligned} [\sigma(\nu_e e)]_{SM+NSI} = & \frac{2G_F^2 m_e}{\pi} T^{\max} [(\tilde{g}_{eL} + 1)^2 + \sum_{\alpha \neq e} |\varepsilon_{\alpha e}^{eL}|^2 \\ & + \left((\tilde{g}_{eR})^2 + \sum_{\alpha \neq e} |\varepsilon_{\alpha e}^{eR}|^2 \right) \left(1 - \frac{T^{\max}}{E_\nu} + \frac{1}{3} \left(\frac{T^{\max}}{E_\nu} \right)^2 \right) \\ & - \left((\tilde{g}_{eL} + 1) \tilde{g}_{eR} + \sum_{\alpha \neq e} \text{Re}[(\varepsilon_{\alpha e}^{eL})^* \varepsilon_{\alpha e}^{eR}] \right) \frac{m_e T^{\max}}{2E_\nu^2}] \end{aligned} \quad (13)$$

and

$$\begin{aligned} [\sigma(\nu_{\mu,\tau} e)]_{SM+NSI} = & \frac{2G_F^2 m_e}{\pi} T^{\max} [\tilde{g}_{\mu,\tau L}^2 + \sum_{\alpha \neq \mu,\tau} |\varepsilon_{\alpha \mu,\tau}^{eL}|^2 \\ & + \left(\tilde{g}_{\mu,\tau R}^2 + \sum_{\alpha \neq \mu,\tau} |\varepsilon_{\alpha \mu,\tau}^{eR}|^2 \right) \left(1 - \frac{T^{\max}}{E_\nu} + \frac{1}{3} \left(\frac{T^{\max}}{E_\nu} \right)^2 \right) \\ & - \left(\tilde{g}_{\mu,\tau L} \tilde{g}_{\mu,\tau R} + \sum_{\alpha \neq \mu,\tau} \text{Re}[(\varepsilon_{\alpha \mu,\tau}^{eL})^* \varepsilon_{\alpha \mu,\tau}^{eR}] \right) \frac{m_e T^{\max}}{2E_\nu^2}], \end{aligned} \quad (14)$$

where

$$\tilde{g}_{\alpha R} = \sin^2 \theta_w + \varepsilon_{\alpha\alpha}^{eR} \text{ and } \tilde{g}_{\alpha L} = \sin^2 \theta_w - \frac{1}{2} + \varepsilon_{\alpha\alpha}^{eL}, \quad (15)$$

and m_e is the electron mass, E_ν is the neutrino energy and T^{\max} is the maximum of the recoiled-electron energy in the detector, $T^{\max}(E_\nu) \equiv E_\nu / (1 + m_e/2E_\nu)$, where $0 < E_\nu < 0.420$ MeV for pp events and $E_\nu = 0.862$ MeV and 1.44 MeV for ${}^7\text{Be}$ and pep events respectively.

The factors $\text{Re}[(\varepsilon_{\alpha e}^{eL})^* \varepsilon_{\alpha e}^{eR}]$ and $\text{Re}[(\varepsilon_{\alpha \mu,\tau}^{eL})^* \varepsilon_{\alpha \mu,\tau}^{eR}]$ can be written equivalently as $|\varepsilon_{\alpha e}^{eL}| |\varepsilon_{\alpha e}^{eR}| \cos(\phi_{\alpha e}^{eL} - \phi_{\alpha e}^{eR})$ and $|\varepsilon_{\alpha \mu,\tau}^{eL}| |\varepsilon_{\alpha \mu,\tau}^{eR}| \cos(\phi_{\alpha \mu,\tau}^{eL} - \phi_{\alpha \mu,\tau}^{eR})$, respectively, in terms of the magnitudes and CP-violating phases, $\phi_{\alpha\beta}^{eL,R}$, [37, 38, 42, 43] of the complex, FC parameters.

III. PP , ${}^7\text{Be}$ AND PEP EXPECTED EVENT RATES AT BOREXINO

The basic input for the event rate calculation requires the flux of neutrinos at Earth, the number of electron targets in the fiducial volume of the detector, the cross section for $\nu + e \rightarrow \nu + e$ elastic scattering⁴ and the exposure time. In Borexino the results are typically presented as a rate per 100 tons of detector per day. The pp result requires the convolution of the relevant cross section and the pp energy spectrum [6, 44], whereas the other two cases are line spectra and involve only the product of total flux and the cross section at production energy. All the Borexino low-energy papers [6–8] use the high-metallicity total solar fluxes emitted as calculated by Serenelli, Haxton and Peña-Garay [45] for reference values in their quoted “expected count rate” estimate in each case. We follow suit in our rate estimates for χ^2 tests of parameter best-fits and limits.⁵

A. Estimate of matter effects on the ν_e survival probability

The pp continuous energy flux distribution of emitted neutrinos, $\phi(E_\nu)_{pp}$, is outlined in the Appendix. For these lowest-energy neutrinos ($E_\nu \leq 0.420$ MeV), the matter effects on the probability P_{ee} that a ν_e survives the trip from

⁴ Unless indicated otherwise, we use the current Z-pole \overline{MS} value of $\sin^2(\theta_W)$ in cross section evaluations.

⁵ The pep rate uncertainties are not Gaussian [8]. Nonetheless we use the nominal values given in Table I of Ref. [8] to estimate the weight of the pep data in our various fits.

the Sun's core to the detector are very small, less than a percent different from the path-averaged, pure vacuum-mixing prediction. For the somewhat higher, single energy ${}^7\text{Be}$ (0.862 MeV) and pep (1.44 MeV) neutrinos, the matter effects are still small, 4-5%, but not entirely negligible. For all three sources, we include the small corrections due to matter effects to the pure vacuum value of $\langle P_{ee} \rangle$. The NSI matter effects on the pp spectrum are negligible [46] and therefore not included. Because the NSI propagation corrections to the LMA-MSW model [41, 47–49] for P_{ee} will be small corrections to small effects below 2 MeV [13] and our CC semi-leptonic source NSI do not enter the matter effects, and, as with the pp spectral shape, we do not include the remaining matter contributions from the ν -e forward scattering process in this paper⁶.

The cross sections are those for neutrino-electron scattering defined in Sec. II D, the number of electrons per 100 tons of target, $N_e = 3.307 \times 10^{31}$ and the pp flux as summarized in the Appendix in Eq. (19) and Eq. (20). For the ${}^7\text{Be}$ and pep fluxes, which have discrete energy spectra, we treat the fluxes as delta functions in evaluating the rate in Eq. (16). Following Borexino, we take the high-metallicity SSM flux values $\phi_{{}^7\text{Be}} = 4.48 \times 10^9 \text{ cm}^{-2}\text{s}^{-1}$ at 0.862 MeV and $\phi_{pep} = 1.44 \times 10^8 \text{ cm}^{-2}\text{s}^{-1}$ at 1.44 MeV to compute our “expected values”. To incorporate the mild energy dependence in the ${}^7\text{Be}$ and pep cases, we use the analytic LMA-MSW matter dependence outlined in the “Neutrino mixing” review in Ref. [41] for P_{ee} and for $\cos\theta_{12}$. As for the pp case, we use electron density at average pp neutrino production point in these expressions, determined by taking the average production distance from the solar core [50] and then assuming an exponential decrease in density outward from the core in the analytic approximations.

In summary, we find that the modifications to the straight energy-independent vacuum value of $\langle P^{vac} \rangle_{ee} = 0.558$ give the values $\langle P^{pp} \rangle_{ee} = 0.554$, $\langle P^{7\text{Be}} \rangle_{ee} = 0.536$ and $\langle P^{pep} \rangle_{ee} = 0.529$. We use these values in our evaluation of production rates to compare to the Borexino values and to set limits on parameters. The basic structure of the expected rate calculations reads

$$R_\nu^i = N_e \int_0^{E_{max}} dE_\nu \phi^i(E_\nu) \left(\sigma_e(E_\nu) \langle P^i \rangle_{ee} + \sigma_{\mu,\tau}(E_\nu) [1 - \langle P^i \rangle_{ee}] \right), \quad (16)$$

where $\langle P^i \rangle_{ee}$ are given in Eq. (11), with the index i indicating whether vac , pp , ${}^7\text{Be}$ or pep is inserted for the factor $\langle P \rangle_{ee}^{SMM}$ in the application. The cross sections $\sigma_e(E_\nu)$ and $\sigma_{\mu,\tau}(E_\nu)$ are defined in Eq. (13) and Eq. (14). The effects of the MSW-LMA model are small, but we find that they do make noticeable difference in details of the fits. To test a model where matter effects play no role at the lowest energies, one simply adopts the energy-independent “vac” value for $\langle P \rangle_{ee}$.

IV. THE STANDARD MODEL: LOW-ENERGY FIT TO $\sin^2(\theta_W)$

There is ongoing interest in the low-energy determination of the weak-mixing angle $\sin^2(\theta_W)$ [20, 51]. Presently the lowest energy determination of the weak-mixing parameter $\sin^2(\theta_W)$ is that provided by the parity-violation measurement in ${}^{133}\text{Cs}$ at 2.4 MeV [52–54]. Current and future solar neutrino measurements at the pep energy and below can test the $\sin^2(\theta_W) = 0.23867 \pm 0.00016$ prediction of \overline{MS} running of this parameter to the sub-MeV region [55].

With all NSI parameters set to zero in our theoretical rate Eq. (16), we fit $\sin^2(\theta_W)$ and determine its uncertainty with the straightforward χ^2 estimator

$$\chi^2(\sin^2(\theta_W)) = \sum_i \frac{(R_\nu^i(\sin^2(\theta_W)) - R_{exp}^i)^2}{(\sigma_{exp}^i)^2}, \quad (17)$$

where i runs over the solar neutrino sources pp , ${}^7\text{Be}$ and pep and where the expression for the phenomenological rate is given in Eq. (16). With all NSI parameters set to zero and the PDG(2016) [41] value $\sin^2(\theta_W) = 0.2313$, our expected rate values are $R^{pp} = 132$ (144 ± 13 [6]), $R^{7\text{Be}} = 48.2$ (46 ± 1.5 [7]) and $R^{pep} = 2.85$ (3.1 ± 0.6 [8]), where the Borexino measured values are given in parentheses after each expected rate value. The expected value of the rate is

⁶ Using global data on neutrino propagation through Earth, neglecting ν -e NSI in matter and at detectors, Ref. [14] finds that NC semileptonic NSI improve the fit to the energy dependence of P_{ee} in the 2 MeV to 10 MeV transition region.

larger than the measured value in the ${}^7\text{Be}$ case, so one expects the fit will result in a smaller value of the weak-mixing angle. Because the relative error is significantly smaller in this measurement, it will have the largest impact on the combined fit.

Using Borexino's published values for the rates and their 1σ statistical uncertainties for pp , ${}^7\text{Be}$ and pep direct detection, we find a best-fit $\sin^2(\theta_W) = 0.224 \pm 0.016$, consistent with both the \overline{MS} value at the Z-boson mass and the low-energy theoretical prediction [55]. As described above in Sec. III A, we use the SMM with the LMA-MSW energy dependence as reviewed in Ref. [41] and include the effect of differing solar electron density at the average production point for each ν_e source. Our result is also consistent with values based on decay and reactor data studies [18–21, 24, 54]. Our central value and uncertainty, which reflects only statistical fluctuations, are somewhat smaller than those of the reactor data alone. *With the inclusion of the pp data, our value is below the energies of all other determinations of the weak-mixing angle to date.*

In Fig. 1, we show the $\Delta\chi^2$ distribution for the three individual spectra and for the combined fit. The 90% C.L. and 1σ values are indicated by the dashed lines. The results of all the four cases are given in Table I. Clearly, the fit is dominated by the ${}^7\text{Be}$ data with its 3% uncertainty, compared to 9% for pp and 19% for pep , whose large uncertainty results in the obvious insensitivity to $\sin^2(\theta_W)$ at very small values, where only the CC contributes. In the pp and ${}^7\text{Be}$ cases, the insensitivity shows up as a slight asymmetry in the limits, with the lower limits being marginally weaker than the upper limits.

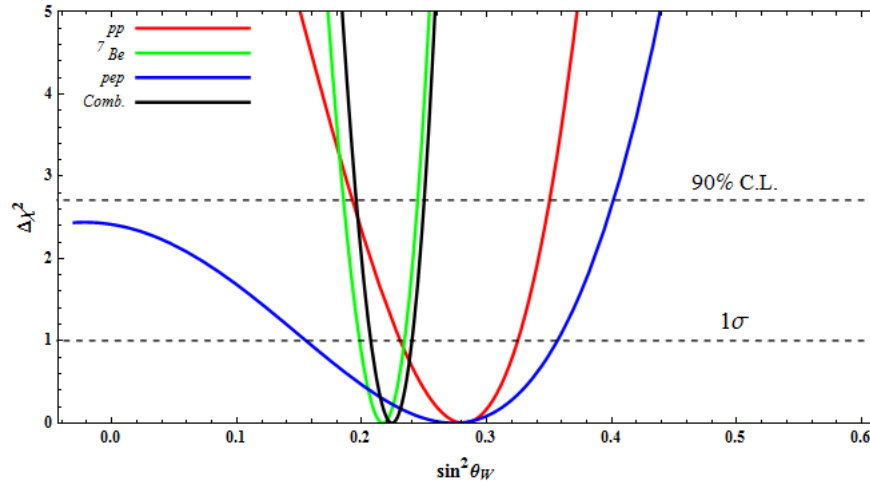


FIG. 1: The SM $\sin^2(\theta_W)$ fit using the solar low-energy spectrum of pp , ${}^7\text{Be}$, pep reaction measured by Borexino experiment. From bottom to top, the 1σ and 90%C.L. bands are shown. The marked asymmetry in the bound from pep data is explained in the text.

Spectrum	Weak Mixing Angle
pp	0.281 ± 0.047
${}^7\text{Be}$	0.217 ± 0.018
pep	0.274 ± 0.101
combined	0.224 ± 0.016

TABLE I: Shown are the $\sin^2(\theta_W)$ fits to individual and combined Borexino low-energy solar neutrino rates. Uncertainties shown are averages of upper and lower values. The preference for a low value of $\sin^2(\theta_W)$ results from the relatively small uncertainty in the ${}^7\text{Be}$ data. The text develops this point.

Another way to look at the the pattern of individual and joint fits is by inspection of the P_{ee} values determined by the Borexino data compared to MSW-LMA expectation as summarized in "Extended Data Figure 2" in Ref. [6], which shows P_{ee} vs. E_ν . The pp and pep experimental points would like a larger value of $\sin^2(\theta_W)$, increasing the cross section in the rate and permitting a smaller P_{ee} while the ${}^7\text{Be}$ point would like a smaller value, permitting a larger P_{ee} value. The small error on the ${}^7\text{Be}$ point gives it more weight, and it pulls the fit down below the input

value. All the data are within 1σ of the curve, so the effects are weak and our average final fit value is consistent with the high energy precision value as well as with other reported low-energy fits to decay and scattering data cited above.

V. NSI AT THE SOURCE (SUN)

The detector NSI are strongly correlated among themselves. The reasons lie in the P_{ee}^{NSI} probability dependence on the NSIs, Eq. (11), and in the structure of the event rate, Eq. (16), which shows the dependence of the rate on the electron survival probability and the cross sections, Eqs. (13,14), on the NSI parameters. When the ε parameters vary and change $\langle P_{ee} \rangle$, they change $1 - \langle P_{ee} \rangle$ in the opposite direction. For example, the coefficients of ε_+ and ε_- in Eq. (11) are both negative, with the latter's magnitude twice that of the former. When they have the same sign, they lower the value of P_{ee}^{NSI} as they grow and raise it as they shrink. The value of $1 - P_{ee}^{NSI}$ then compensates by shrinking or growing. When the values of ε_+ and ε_- have opposite sign and grow in magnitude, they cancel each other and tend to leave the rate unchanged, which leaves the χ^2 unchanged, again leading to degeneracy. When combined with the variations of detector NSI parameters, the situation improves, but long, narrow regions of parameter space can still remain unbounded in some cases. The larger the data set and/or the smaller the uncertainties in the data, the less the impact of these degeneracies on the results of NSI searches.

NSI variations then make the system prone to the extended "filaments" of same-likelihood regions. The large excursions to values greater than one are a result of the rather large uncertainties in the data and our truncation to linear order in the source parameters, which drops the quadratic terms in the FC NSI and the overall normalization factor that ensures that the total probability is constrained to 1.

The regions of parameter space in the neighborhood of the origin, captured by the 1-parameter bounds, are useful as indications of the tightest possible constraints with the given data. We restrict ourselves to these regions for application of the Borexino pp , ${}^7\text{Be}$ and pep data to source NSI bounds in this section. In the presentation of future prospects in Section VII we will return to the question of correlations among NSI parameters.

Setting all of the NSI parameters at the detector equal to zero, we look at the ranges of the $\text{Re}[\varepsilon_{ee}]$, $|\varepsilon_{ee}|$, ε_+ and ε_- parameters allowed by one-parameter-at-a-time fits to the experimentally measured values of the Borexino event rates for pp , ${}^7\text{Be}$ and pep solar neutrino rates. The parameter $\text{Re}[\varepsilon_{ee}]$, the real part of ε , enters linearly in the fit, which restricts its value more tightly than its modulus, which enters quadratically. In effect the modulus bound restricts the value of $\text{Im}[\varepsilon_{ee}]$, because of the separate, tighter linear constraint on $\text{Re}[\varepsilon_{ee}]$. The constraints can then be presented separately in our results that follow.

Figure 2 shows the results of all of the possible one-parameter fits with the oscillation probability formula as given in Eq. (11) and Eq. (12), where the independent NSI parameters are $\text{Re}[\varepsilon_{ee}]$, $|\varepsilon_{ee}|$, ε_+ and ε_- in Fig. 2. Figure 2 clearly shows that the fit is about twice as sensitive to ε_- as it is to ε_+ , which reflects the fact that the coefficient multiplying ε_- is about twice as large as that multiplying ε_+ in Eq. (11).

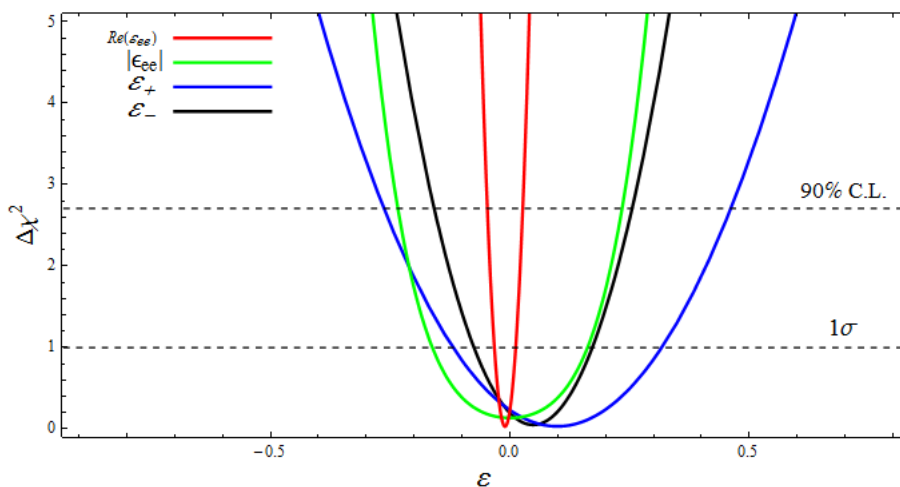


FIG. 2: Source NSI one parameter fits with the 1- σ or 68% C.L. and 90% C.L. levels indicated by the horizontal dashed lines. The corresponding best-fit values and 90% C.L. spread is shown in Table II

With all other parameters set to zero, the 90% C.L. one parameter bounds on the source parameters are listed in Table II. These generally compare reasonably well with bounds from other data and global fits to solar data from

NSI Para.	$\text{Re}[\varepsilon_{ee}]$	$ \varepsilon_{ee} $	ε_+	ε_-
Best-Fits	-0.0163	0.0	0.158	0.082
Bounds	[-0.038, 0.038]	[-0.223, 0.223]	[-0.370, 0.370]	[-0.212, 0.212]

TABLE II: 1-parameter source NSI parameter best fit values and their corresponding 90% C.L. uncertainties.

other NSI studies. For example, comparing to Table II in Ref. [18], we find $-0.72 \leq |\varepsilon_{ee}| \leq 0.72$ and similarly for $\varepsilon_{e\mu}$ and $\varepsilon_{e\tau}$ at 90% C.L., while the corresponding allowed ranges given in Table II are about half that.

To make contact between bounds on $\varepsilon_{+/-}$ and bounds on the NSI parameters $\varepsilon_{e\mu}$ and $\varepsilon_{e\tau}$, we display the definitions from Eq. (12) here.

$$\begin{aligned} c_{23}\varepsilon_+ &\equiv \left| \varepsilon_{e\mu}^{udL} \right| \cos(\phi_{e\mu} + \delta_{CP}) s_{23} + \left| \varepsilon_{e\tau}^{udL} \right| \cos(\phi_{e\tau} + \delta_{CP}) c_{23} \\ c_{23}\varepsilon_- &\equiv \left| \varepsilon_{e\mu}^{udL} \right| \cos \phi_{e\mu} c_{23} - \left| \varepsilon_{e\tau}^{udL} \right| \cos \phi_{e\tau} s_{23} \end{aligned}$$

The relationships are complicated by the dependence on the phases $\phi_{e\mu}$, $\phi_{e\tau}$ and δ , but simplify greatly when $\delta = 0$ or π . For example, when $\delta_{CP} = 0$, only the real parts of $\varepsilon_{e\mu/\tau}$ appear. Therefore the ε_+ nonzero and $\varepsilon_- = 0$ converts to the statement

$$\text{Re}(\varepsilon_{e\mu}) \approx \text{Re}(\varepsilon_{e\tau}) \approx \frac{1}{2}\varepsilon_+, \quad (18)$$

and similarly when only $\varepsilon_- \neq 0$ and all other NSI = 0. The approximate relationships become exact when $\tan(\theta_{23}) = 1$. In short, the bounds on the $\varepsilon_{e\mu,\tau}$ parameters are about twice as tight as those listed for the $\varepsilon_{+/-}$ parameters. If it turns out that $\delta \approx \frac{3\pi}{2}$, the current best-fit of value of δ_{CP} in the SMM scenario, however, no such simple connection can be made, since the ε_+ parameter is related to the imaginary parts of the $\varepsilon_{e\mu,\tau}$ parameters. Nonetheless we include the $\delta = 0$ example to indicate that the constraints on one set of parameters lead to similar constraints on the other.

The range allowed by early, model-independent surveys like [56] are significantly tighter than those we find from the current Borexino data, however, where bounds set by CKM unitarity are $|\varepsilon_{ee}| \approx |\text{Im}[\varepsilon_{ee}]| \leq 0.041$, and likewise for $\varepsilon_{e\mu,\tau}$.⁷ We note that the best-fit value for ε_- implies a value 0.041 for $\varepsilon_{e\mu,\tau}$, just at the 90% C.L. limit quoted in [56]. Our limits on this value are broad, but it is interesting to see that a fit preferring this value is not ruled out. The bound quoted from [56] is based on nuclear decay rates and is independent of the values of the neutrino mixing parameters, whereas an input to our bound is the value $\sin^2 \theta_{12} = 0.297$ from Ref. [?].

A detailed NSI study using Borexino precision ⁷Be data [40] considers only the leptonic NSIs involved at the detector, assuming all matter and source effects are negligible. We will comment on this study in connection with our NSI at detector analysis next.

VI. NSI AT THE BOREXINO DETECTOR

Here we turn to the sensitivity of the detector NSIs to the low-energy solar data when all of the source NSIs are set equal to zero. Again, since the matter effects in the LMA-MSW model are 4% – 5% at E_ν values from the ⁷Be and *pep* sources, we include this energy variation [41] in calculating the expected rates when NSIs at the detector are active. As remarked earlier, we note that the NSI contributions to the matter effects at low-energy are small [13], so the standard LMA-MSW description suffices.⁸

⁷ Bounds on quark-neutrino NSI from matter effects alone, for example [14, 15], bound NC-type NSI and are not relevant to our CC NSI study.

⁸ For a solar model independent check of the LMA-MSW, see Ref. [49].

A. NSIs in the $\nu_e e$ -scattering at the Borexino detector

In this section we show and discuss the 68%, 90% and 95% C.L. boundaries of the independent combinations of detector NSI $\varepsilon_{\alpha\beta}^{eL,R}$ parameters in Fig. 3, where the stars show the locations of the best-fit points closest to the no-NSI points at (0, 0) in each case.⁹ As expected, the data is more sensitive to the left-handed (LH) NSI than to the right-handed (RH) NSI, opposite to the case for reactor $\bar{\nu}_e$ fluxes, where the roles of R and L are reversed compared to the solar ν_e flux [18, 19].

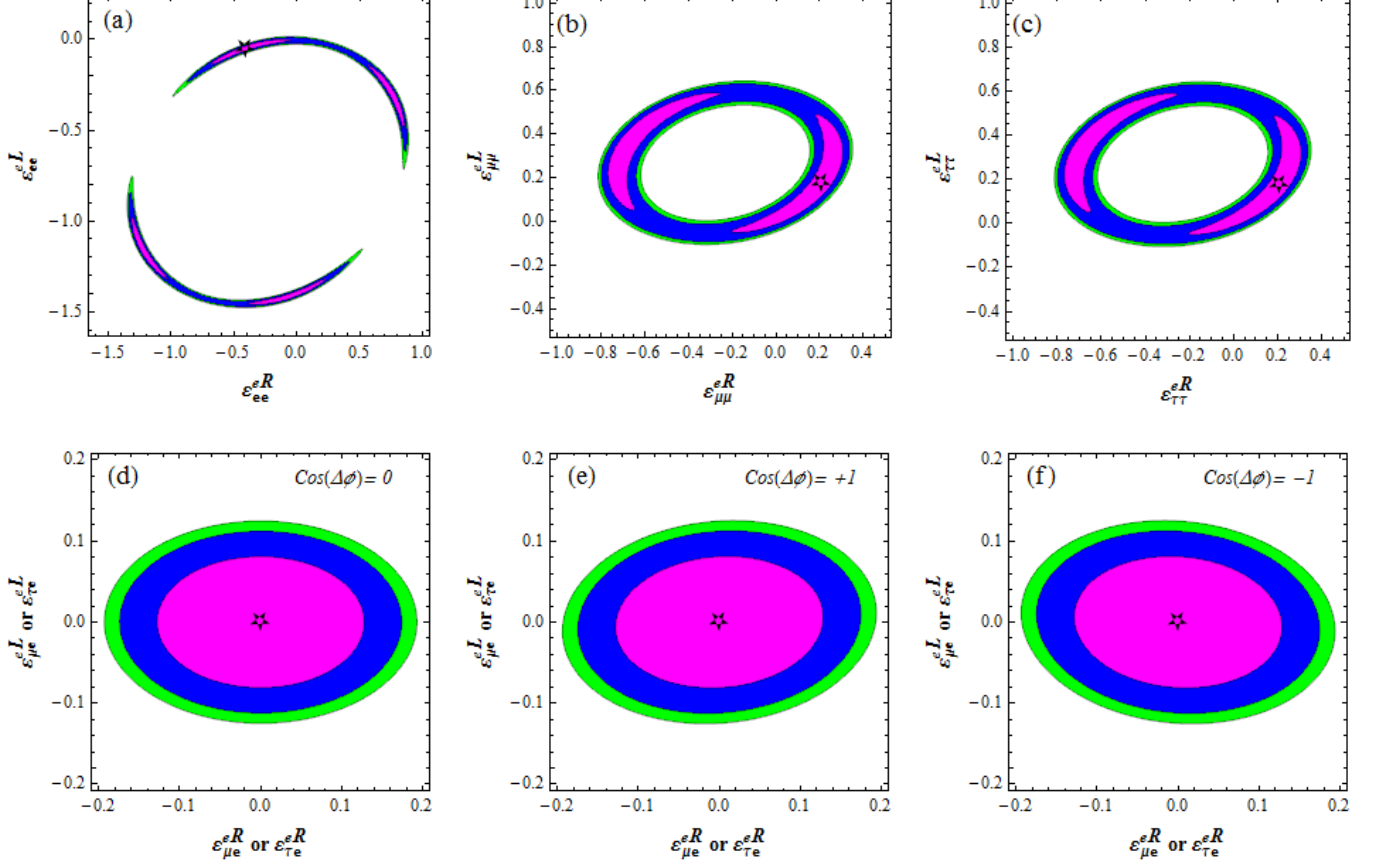


FIG. 3: Allowed 68%(magenta), 90% (blue) and 95% (green) C.L. joint parameter correlations of the NU and FC LH and RH subspaces for NSIs at the detector. The star indicates the “best-fit” point for orientation in each panel. The “no-NSI” point is at the origin, which is also the best fit point for panels d, e and f.

In the second row, the three cases correspond to the NSI phase choices, see Eq.13 and Eq.14, $\cos(\phi_{ae}^{eL} - \phi_{ae}^{eR}) = 0, -1$ and $+1$, from left to right. The sense of the correlations in the cases $\cos(\phi_{ae}^{eL} - \phi_{ae}^{eR}) = +1/-1$ are the same as in the $\bar{\nu}$ detection of reactor neutrinos [18], but the constraint on $\varepsilon_{\alpha\beta}^{eL}$ is now tighter than that on $\varepsilon_{\alpha\beta}^{eR}$, since the roles of the dominant vs. subdominant terms in the cross section are reversed. The relationship $\varepsilon_{\alpha\beta}^{eR,L} = (\varepsilon_{\beta\alpha}^{eR,L})^*$, mentioned in Sec. II A, and the dependence of the cross sections, Eq. 13 and Eq. 14, on only the moduli of the FC NSI parameters and on the cosine of their phase differences lead to identical bounds for the $\varepsilon_{\mu,\tau e}^{eL,R}$ and the $\varepsilon_{e\mu,\tau}^{eL,R}$ NSI parameters. We choose to display the bounds for the former case in Fig. 3. Likewise, the μ and τ labels always appear symmetrically, so their figures are the same.

⁹ There are degenerate best-fit points in panels a, b and c in each of the isolated, 1- σ regions. The (0,0) no-NSIs’ point is in or at the boundary of the 1- σ region in each case.

The two-parameter 90% C.L. boundaries shown in Fig. 3 contain one and two parameter bounds on the corresponding parameters, as summarized in Table III. Our leptonic NSI bounds listed in Table III are comparable to the

Sub-figure no.	1-parameter (LH)	1-parameter (RH)	2-parameters (LH)	2-parameters (RH)
3(a)	$\epsilon_{ee}^{eL} \in [-0.017, 0.027]$	$\epsilon_{ee}^{eR} \in [-0.33, 0.25]$	$\epsilon_{ee}^{eL} \in [-0.55, 0.02]$	$\epsilon_{ee}^{eR} \in [-0.80, 0.90]$
3(b)	$\epsilon_{\mu\mu}^{eL} \in [-0.040, 0.04]$	$\epsilon_{\mu\mu}^{eR} \in [-0.10, 0.12]$	$\epsilon_{\mu\mu}^{eL} \in [-0.61, 0.15]$	$\epsilon_{\mu\mu}^{eR} \in [-0.33, 0.86]$
3(d)	$\epsilon_{\mu e}^{eL} \in [-0.153, 0.153]$	$\epsilon_{\mu e}^{eR} \in [-0.238, 0.238]$	$\epsilon_{\mu e}^{eL} \in [-0.152, 0.152]$	$\epsilon_{\mu e}^{eR} \in [-0.231, 0.231]$
3(e)	$\epsilon_{\mu e}^{eL} \in [-0.152, 0.152]$	$\epsilon_{\mu e}^{eR} \in [-0.236, 0.236]$	$\epsilon_{\mu e}^{eL} \in [-0.156, 0.156]$	$\epsilon_{\mu e}^{eR} \in [-0.244, 0.244]$
3(f)	$\epsilon_{\mu e}^{eL} \in [-0.152, 0.152]$	$\epsilon_{\mu e}^{eR} \in [-0.236, 0.236]$	$\epsilon_{\mu e}^{eL} \in [-0.156, 0.156]$	$\epsilon_{\mu e}^{eR} \in [-0.244, 0.244]$

TABLE III: Parameter bounds from the detector-only study, with both 1-parameter and 2-parameter bounds given here at the 90% C.L.. As noted in the text, the 2-parameter bounds for cases (a), (b) and (c) lie partly outside the range where they can be considered perturbations on the SMM, they are given here for completeness. In all entries, the index μ can be replaced by τ and the e and μ subscripts interchanged.

comprehensive 90% bounds for one parameter at-a-time from Ref. [19], Table 5, determined from global low-energy reactor data. Compared to the bounds cited in [57], Table 3, the ϵ_{ee}^{eL} and $\epsilon_{\tau e}^{eL}$ bounds are tighter, the $\epsilon_{\tau e}^{eR}$ bound is the same and the ϵ_{ee}^{eR} and $\epsilon_{\mu e}^{eL,R}$ bounds are weaker. Overall the bounds we present are similar to the corresponding ones cited in Ref. [57].

For present discussion, there are no comparisons with the results of Ref. [14], which does not include the leptonic NSIs in its analysis, but we can check against Ref. [40]. Their bounds are: $\epsilon_{ee}^{eL} [-0.046, 0.053]$, $\epsilon_{ee}^{eR} [-0.206, 0.157]$, $\epsilon_{\tau\tau}^{eL} [-0.231, 0.866]$, and $\epsilon_{\tau\tau}^{eR} [-0.976, 0.726]$, which are weaker, stronger, weaker and weaker than our corresponding bounds. These comparisons and others we present are meant to be rough indicators of where our work stands in relation to other NSI work, not a serious indication of "best bounds". The variation in the level of treatment of theoretical and experimental uncertainties varies too much among various quoted bounds to make direct, clear-cut comparisons among published bounds.

We will see in the following section on future prospects that the degeneracy effects are under control in most cases, though excursions into unrealistically large perturbation regions, even at one sigma, are still possible.

VII. FUTURE PROSPECTS FOR SUB-MEV DETERMINATION OF $\sin^2(\theta_W)$ AND FOR IMPROVED BOUNDS ON NSI PARAMETERS FROM LOW-ENERGY SOLAR NEUTRINOS

A number of "Borexino-inspired" ideas for experiments have been advanced and proposals made to measure pp and other low-energy neutrinos to a precision of 1% or better. The objectives include determination of the correct solar metallicity model and the corresponding fluxes of photons and neutrinos, stringent testing of the LMA-MSW model of neutrino propagation in the sun, and refined searches for exotic neutrino properties. A number of dark-matter search proposals are reviewed in Ref. [25], where the emphasis is on their high efficiency for identifying and rejecting solar neutrinos, thus providing a 1%-3% precision sample of solar neutrino data, depending on the particular proposal. There are also dedicated solar neutrino proposals such as Ref. [29] that aim for the same level of precision. With these prospects in mind, we present estimates of the improvement in sub-MeV measurement of $\sin^2(\theta_W)$ and NSI parameter space boundaries that would follow from the improved precision.

A. Determination of the low-energy solar value of $\sin^2(\theta_W)$

For the purpose of framing a test, we assume that the true value of the weak-mixing angle is the high energy determination quoted in the PDG-2016 edition, 0.2313. With 1% uncertainties in the measurements of pp , ${}^7\text{Be}$ and pep rates, we ask at what level of confidence is it consistent with the value 0.2387 predicted by SM renormalization group running down to 10 -100 MeV [54, 55] from the high energy measured values? In Fig. 4, we show the results of an estimate of $\Delta\chi^2$ values as a function of $\sin^2(\theta_W)$. By eye one can see that the two values for $\sin^2(\theta_W)$ agree at a $\Delta\chi^2$ of about 5, or about 98% C.L.. Though our estimate is rough, not including input parameter uncertainties, it indicates that new, precision solar measurements have the potential to give useful information about the value of this fundamental parameter at energies an order of magnitude below those currently explored [54].

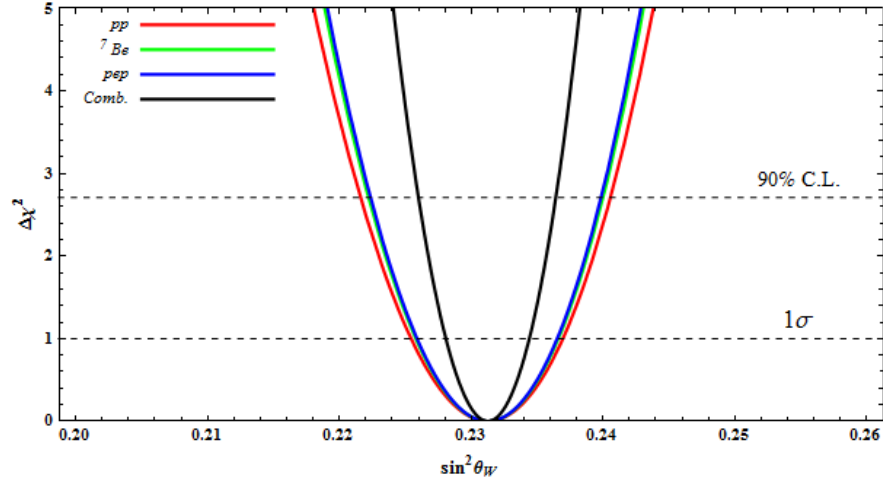


FIG. 4: **Future Prospects:** Low energy solar neutrinos fit to SM $\sin^2(\theta_W)$. From bottom to top, the 1σ and 90% C.L. bands are shown. The experimental rates are assumed to be those of the standard model with $\sin^2(\theta_W)$ set to the \overline{MS} value at the Z-boson mass. At 5σ the allowed value of $\sin^2(\theta_W)$ ranges up to 0.2382.

B. NSI at the source (Sun)

Taking a 1% nominal uncertainty on the experimental rate, and taking the LMA-MSW model with neutrino mixing parameters at their PDG [41] central values, we show the correlation between the ε_+ and ε_- parameters over the limited ranges $(-0.10, +0.10)$ in the central panel of Fig. 5. The left panel shows a range of ε_- expanded by a factor of five and the range of ε_+ narrowed to the vicinity around zero. This slice indicates the rapid rise in $\Delta\chi^2$ at small, fixed ε_+ and rising ε_- .

Focussing on the central figure, we see a degenerate trough of low $\Delta\chi^2$ values along a line starting from the right-front corner at about $(0.07, -0.1)$ to the rear corner at about $(-0.03, 0.1)$, along which the contributions from these two source NSIs tend to cancel each other, as discussed in Sec. V. Similarly, the steep slopes along the line from the front left corner at $(-0.1, -0.1)$ to the rear right corner at $(0.1, 0.1)$ show a region along which they add. The right panel shows this pattern blown up in the center of the region covered by the central panel.

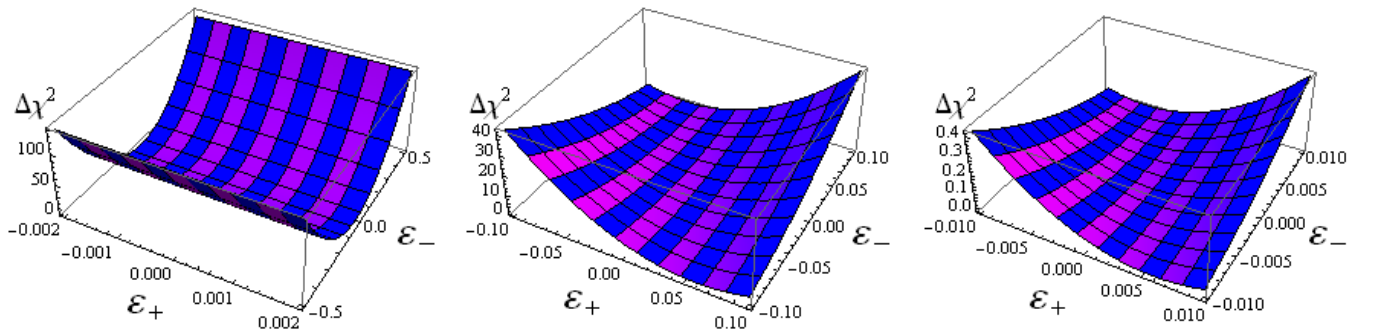


FIG. 5: **Future Prospects:** 3-dimensional view of the correlation between source NSI parameters ε_+ and ε_- . See text for details.

In Fig. 6, we show the individual bounds on all of the source ε parameters at 68% and 90% C.L.. This corresponds to the $\varepsilon_+ = 0$ slice of the left panel of Fig. 5 in the range $-0.10 \leq \varepsilon_- \leq 0.10$. Fig. 6 shows the same qualitative features as Fig. 2, but the bounds on $\text{Re}(\varepsilon_{ee})$, ε_+ and ε_- have been tightened by factors of 4, as indicated in Table IV. As argued

in Sec. V, connecting these bounds with bounds on the FC NSI $\epsilon_{e\mu}$ or $\epsilon_{e\tau}$ suggests that the bounds shown in Table IV for ϵ_+ and ϵ_- should be divided by 2 for estimating the bounds on their flavor-labeled counterparts, making them competitive with or tighter than those currently available in Ref. [56], Table III, and Ref. [57], Table IV, for example.

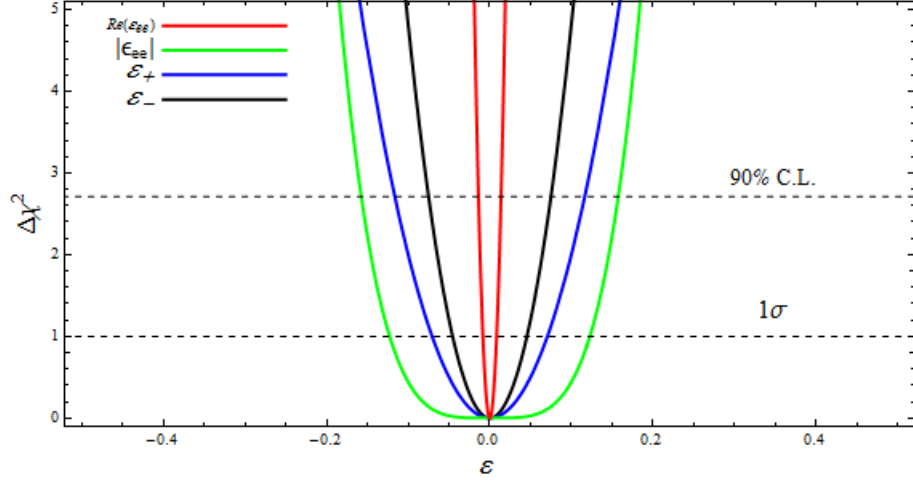


FIG. 6: **Future prospects:** Boundaries on individual source NSI parameters $\epsilon_{+,-}$, $|\epsilon_{ee}|$, and $\text{Re}(\epsilon_{ee})$ are shown with 1σ and 90% C.L. lines. The latter are listed in Table IV

NSI Para.	$\text{Re}(\epsilon_{ee})$	$ \epsilon_{ee} $	ϵ_+	ϵ_-
Best-Fits	0.0	0.0	0.0	0.0
Bounds	$[-0.005, 0.005]$	$[-0.09, 0.09]$	$[-0.05, 0.05]$	$[-0.023, 0.023]$

TABLE IV: **Future Prospects:** 1-parameter at-a-time source NSI parameter bounds at the 90% C.L..

C. NSI at the detector

Following a similar procedure as described in Sec. VI, we explore the two-parameter NSI subspaces and plot the corresponding two-dimensional space boundaries in Fig. 7. Again, the qualitative features are similar to those of the contours shown in the Borexino data-based fits in Fig. 3, but the boundaries are tightened by factors of 4 to 5 in the NU case $\epsilon_{ee}^{eL,R}$ and by factors of two-to-three for the rest of the correlated pairs shown. The complete set of bounds is summarized in Table V.

Sub-fig. no.	1-parameter (RH)	1-parameter (LH)	2-parameters (RH)	2-parameters (LH)
7(a)	$\epsilon_{ee}^{eR} \in [-0.076, 0.084]$	$\epsilon_{ee}^{eL} \in [-0.0046, 0.0046]$	$\epsilon_{ee}^{eR} \in [-0.085, 0.12]$	$\epsilon_{ee}^{eL} \in [-0.0064, 0.0047]$
7(b)	$\epsilon_{\mu\mu}^{eR} \in [-0.02, 0.02]$	$\epsilon_{\mu\mu}^{eL} \in [-0.01, 0.01]$	$\epsilon_{\mu\mu}^{eR} \in [-0.11, 0.12]$	$\epsilon_{\mu\mu}^{eL} \in [-0.042, 0.073]$
7(d)	$\epsilon_{\mu e}^{eR} \in [-0.112, 0.112]$	$\epsilon_{\mu e}^{eL} \in [-0.077, 0.077]$	$\epsilon_{\mu e}^{eR} \in [-0.114, 0.114]$	$\epsilon_{\mu e}^{eL} \in [-0.076, 0.076]$
7(e)	$\epsilon_{\mu e}^{eR} \in [-0.112, 0.112]$	$\epsilon_{\mu e}^{eL} \in [-0.077, 0.077]$	$\epsilon_{\mu e}^{eR} \in [-0.117, 0.117]$	$\epsilon_{\mu e}^{eL} \in [-0.080, 0.080]$
7(f)	$\epsilon_{\mu e}^{eR} \in [-0.112, 0.112]$	$\epsilon_{\mu e}^{eL} \in [-0.077, 0.077]$	$\epsilon_{\mu e}^{eR} \in [-0.117, 0.117]$	$\epsilon_{\mu e}^{eL} \in [-0.080, 0.080]$

TABLE V: **Future Prospects:** Parameter bounds are listed for the detector-only study. τ can be substituted for μ in all entries to obtain the corresponding τ limits. Both 1-parameter and 2-parameter bounds are given here at the 90% C.L..

Comparing the limits illustrated in Fig. 7 and detailed in Table V with those in Eq. (45) of Ref. [56] or with the compilation presented in Table 3 of Ref. [57], we find that in every case our future prospects estimates of detector NSI bounds are up to an order of magnitude tighter than those listed in these reviews. Comparing with the global

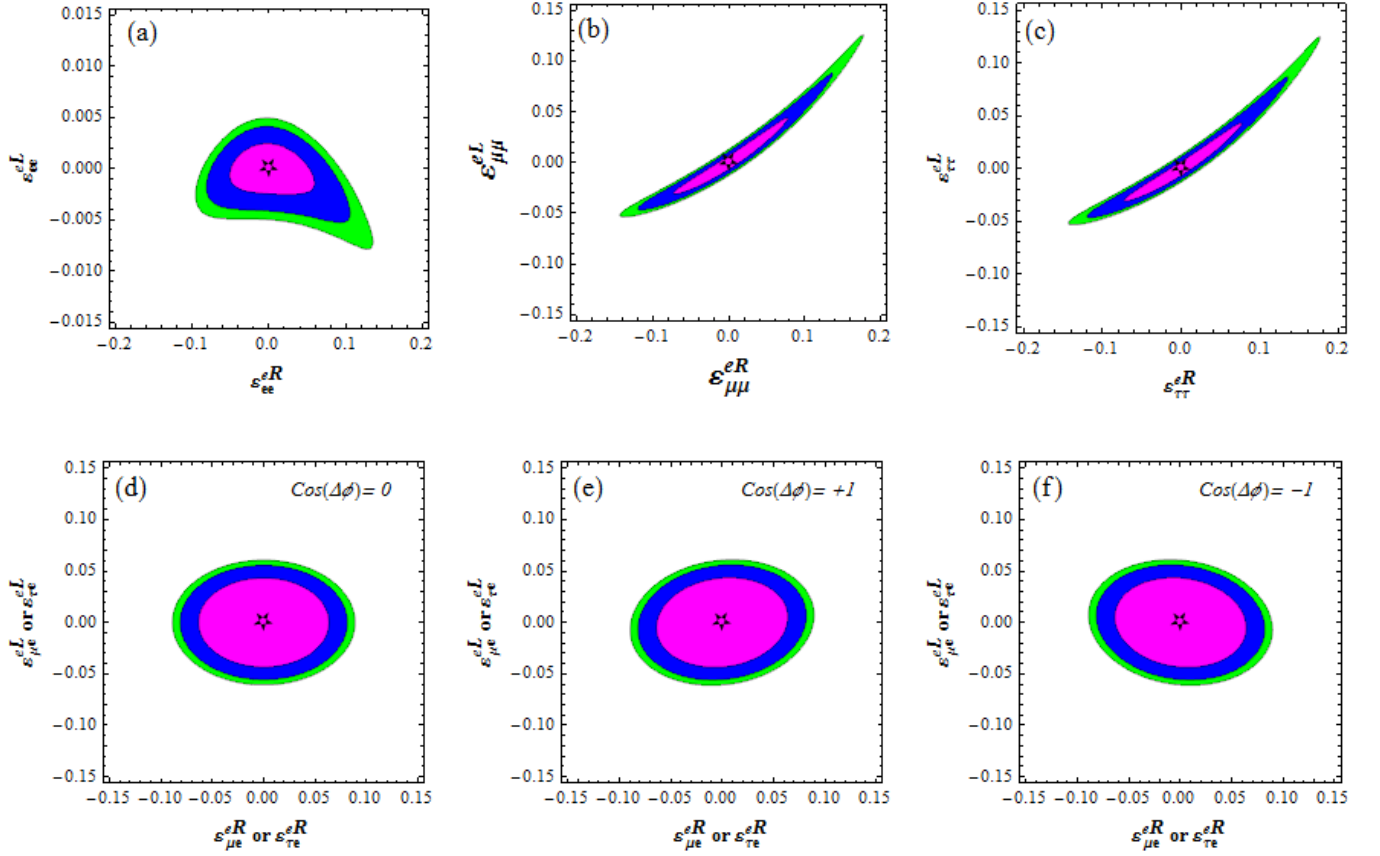


FIG. 7: **Future Prospects:** Allowed 68% (magenta), 90% (blue) and 95% (green) C.L. NSI boundaries are shown for the detector-only case. By definition of the "data" and the χ^2 , the best-fit value, indicated by the star, is at the origin in each case.

analysis of short-baseline neutrino results in Ref. [19], we also find that, with the exception of the ϵ_{ee}^{eR} case, our estimates of the possible extension of the search for new physics go significantly deeper with 1% solar data.

D. Correlation of source and detector NSI parameters

To find correlations between the source and detector NSIs in the case of proposed 1% precision experiments, we study the two-parameter subspaces displayed in Fig. 8. These results show a striking difference between the results for the case of the oscillating long baseline solar experiments and the very short-baseline TEXONO-type experiments. The source vs. detector plots and parameter bound tables contain strong one-parameter limits and strong two-parameter limits on the detector FC NSI in the region of small source parameters, shown in panels (i) through (l), while the TEXONO type experiments leave this region unbounded, as indicated in Fig. 2 of Ref. [18]. The reason is that only direct emission of $\bar{\nu}_\mu$ or $\bar{\nu}_\tau$ from the source can lead to signals in the detector from $\bar{\nu}_\mu$ -e interactions in the latter case, so turning off the NSIs producing $\bar{\nu}_\mu$ at the source eliminates the bound on FC events at the detector. In the solar oscillation case, ν_e from the source can oscillate to ν_μ and contribute signal from these strictly NC type interactions.

Because the effective Lagrangian, Eq.(6), is Hermitian and the cross sections in Eq. (13) and Eq. (14) contain only absolute magnitudes of the FC NSIs and the cosine of the difference of their phases, interchanging flavor labels μ and e leaves the results in the figures and in the tables unchanged. Again the τ and μ results are all the same, so only the latter cases are shown.

The source and detector correlation plots show the features that, as with the source-only study, there are stronger constraints on ϵ_- than on ϵ_+ and on $\epsilon_{e\alpha}^{eL}$ than on $\epsilon_{e\alpha}^{eR}$. They have the distinctive feature of "wings" that are long compared to the compact region around the origin, where the NSI are confined to small deviations from NSIs =

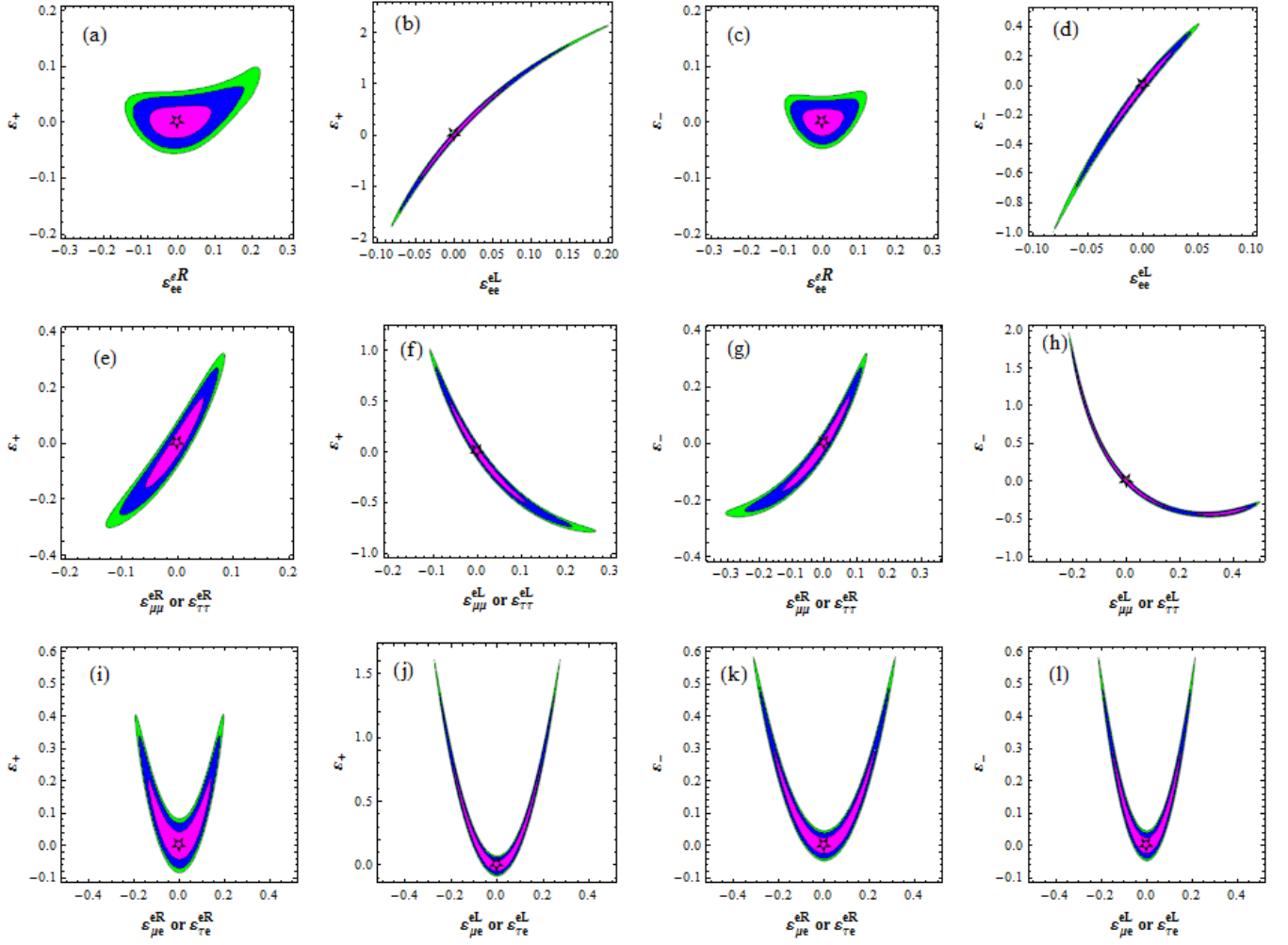


FIG. 8: **Future Prospects:** Future prospect boundaries on combined source and detector NSI parameter correlations at 68% (magenta), 90% (blue), and 95% (green). For the detector FC NSI parameters from (i) to (l), the C.L. regions of $\epsilon_{e\mu}^{eR}$ etc. are the same as those of the parameters shown because of the hermiticity of the leptonic Lagrangian.

0. These tenuous regions of parameter space allow relatively long, highly correlated, excursions from the LMA-MSW picture at 90% C.L. in many cases. These arise from some surprisingly tight correlations between the $\epsilon_{\alpha\beta}^{eR,L}$ contributions to the cross sections at the detector and the $\epsilon_{+,-}$ contributions to P_{ee}^{NSI} from the solar fusion source. For example, take panels 8(b) and 8(f). In panel 8(b), as ϵ_{ee}^{eL} grows it drives growth in $\sigma(\nu_e e)$, while growth in ϵ_{+} drives contraction of P_{ee} . The product $P_{ee} \times \sigma(\nu_e e)$ appears in the rate equation, so there is evidently a highly tuned line of correlated values that allows a long, thin excursion from the best-fit value at the origin to large values of this NSI pair, while still staying within the prescribed confidence levels. A similar situation arises in panel 8(f), but here as $\epsilon_{\mu\mu}^{eL}$ grows it makes $\tilde{g}_{\mu L}$ shrink, which causes $\sigma(\nu_\mu e)$ to shrink. If ϵ_{+} grows, P_{ee} shrinks, but then $1-P_{ee}$ grows and compensates for the shrinking of the ν_μ -e cross section, leading to an anti-correlation as shown in panel 8(f). The situation is similar in the corresponding ϵ_{-} plots 8(d) and 8(h).

In Table VI, we display the complete lists of source and detector two-parameter correlated bounds. The single parameter bounds are the same as found in the corresponding source-only and detector-only studies, as they must be, and the future potential comparisons with published bounds and related discussion presented there applies here, namely that the single parameter bounds show potential for significant improvement in sensitivity to new physics. The range of the correlated 90% C.L. bounds on all of the purely leptonic NSI, those that affect the cross sections that apply at the Borexino detector, are rather tight, consistent with small deviations from the SM values and generally show promise to tighten the bounds listed in TABLE V of Ref. [19]. The correlated bounds (a), (c), (e), (g), (i), (k) and (l) on $\epsilon_{+,-}$ are consistent with the linear approximation assumed in Sec. II C and applied throughout. Even in these

Fig. No.	1-parameter(RH)	1-parameter(LH)	2-parameters(RH)	2-parameters(LH)
8(a)	$\varepsilon_{ee}^{eR} \in [-0.07, 0.07]$	$\varepsilon_+ \in [-0.07, 0.07]$	$\varepsilon_{ee}^{eR} \in [-0.08, 0.11]$	$\varepsilon_+ \in [-0.07, 0.09]$
8(b)	$\varepsilon_{ee}^{eL} \in [-0.004, 0.004]$	$\varepsilon_+ \in [-0.07, 0.07]$	$\varepsilon_{ee}^{eL} \in [-0.075, 0.15]$	$\varepsilon_+ \in [-1.5, 1.8]$
8(c)	$\varepsilon_{ee}^{eR} \in [-0.08, 0.08]$	$\varepsilon_- \in [-0.04, 0.04]$	$\varepsilon_{ee}^{eR} \in [-0.09, 0.10]$	$\varepsilon_- \in [-0.04, 0.04]$
8(d)	$\varepsilon_{ee}^{eL} \in [-0.003, 0.003]$	$\varepsilon_- \in [-0.03, 0.03]$	$\varepsilon_{ee}^{eL} \in [-0.06, 0.043]$	$\varepsilon_- \in [-0.7, 0.37]$
8(e)	$\varepsilon_{\mu\mu}^{eR} \in [-0.022, 0.022]$	$\varepsilon_+ \in [-0.07, 0.07]$	$\varepsilon_{\mu\mu}^{eR} \in [-0.1, 0.07]$	$\varepsilon_+ \in [-0.26, 0.27]$
8(f)	$\varepsilon_{\mu\mu}^{eL} \in [-0.010, 0.010]$	$\varepsilon_+ \in [-0.07, 0.07]$	$\varepsilon_{\mu\mu}^{eL} \in [-0.10, 0.21]$	$\varepsilon_+ \in [-0.75, 0.85]$
8(g)	$\varepsilon_{\mu\mu}^{eR} \in [-0.006, 0.006]$	$\varepsilon_- \in [-0.009, 0.009]$	$\varepsilon_{\mu\mu}^{eR} \in [-0.27, 0.34]$	$\varepsilon_- \in [-0.27, 0.34]$
8(h)	$\varepsilon_{\mu\mu}^{eL} \in [-0.010, 0.010]$	$\varepsilon_- \in [-0.04, 0.04]$	$\varepsilon_{\mu\mu}^{eL} \in [-0.21, 0.49]$	$\varepsilon_- \in [-0.47, 1.8]$
8(i)	$\varepsilon_{\mu e}^{eR} \in [-0.08, 0.08]$	$\varepsilon_+ \in [-0.07, 0.07]$	$\varepsilon_{\mu e}^{eR} \in [-0.18, 0.18]$	$\varepsilon_+ \in [-0.07, 0.34]$
8(j)	$\varepsilon_{\mu e}^{eL} \in [-0.06, 0.06]$	$\varepsilon_+ \in [-0.06, 0.06]$	$\varepsilon_{\mu e}^{eL} \in [-0.25, 0.25]$	$\varepsilon_+ \in [-0.07, 1.3]$
8(k)	$\varepsilon_{\mu e}^{eR} \in [-0.08, 0.08]$	$\varepsilon_- \in [-0.04, 0.04]$	$\varepsilon_{\mu e}^{eR} \in [-0.29, 0.29]$	$\varepsilon_- \in [-0.04, 0.49]$
8(l)	$\varepsilon_{\mu e}^{eL} \in [-0.055, 0.055]$	$\varepsilon_- \in [-0.040, 0.040]$	$\varepsilon_{\mu e}^{eL} \in [-0.20, 0.20]$	$\varepsilon_- \in [-0.04, 0.48]$

TABLE VI: **Future Prospects:** Parameter bounds from the source and detector correlation study. In each entry where μ appears, τ can be substituted with the same range of values for the bounds. Both 1-parameter and 2-parameter bounds are given here at the 90% C.L..

cases, however, the correlations with the leptonic NSIs carry the limits well beyond their single parameter ranges.

In the cases (b), (d), (f), (h) and (j), the ranges of the $\varepsilon_{+,-}$ parameters allowed at 90% C.L. reach well beyond linear approximation values. To treat them consistently requires that the P_{ee} expressions complete to quadratic order be employed. This goes beyond the scope of the present work, which takes a first look at the role of NSIs at the source in the low-energy range of solar neutrinos, where matter effects are very small, as our estimates show, and the semi-leptonic NSIs that apply to the pp , ${}^7\text{Be}$ and pep processes are competitive.

E. Correlations among NSI and oscillation parameters

The neutrino-electron cross sections themselves involve the oscillation parameters only indirectly through the rate calculation, so the focus is on the source parameters. These are directly entangled with the mixing parameters through the ν_e arrival factor $\langle P \rangle_{ee}^{NSI}$ in Sec. IIC. For our case, θ_{23} is involved only in the definitions of ε_+ and ε_- , which relate them to $\varepsilon_{e\mu}$ and $\varepsilon_{e\tau}$, so it ties only indirectly to other experiments. The mass-squared difference $m_2^2 - m_1^2$ enters only in the small, matter-effect corrections and our results are insensitive to this parameter. Moreover, in reactor neutrino applications such as the JUNO experiment, where semileptonic NSI are involved at both source and detector, the fits to simulated data that include NSI show little impact on $m_2^2 - m_1^2$ best fits [36].

The situation is quite different for θ_{12} and θ_{13} , which largely determine the coefficients of ε_- and ε_+ , leading to ambiguity in the interpretation of data in terms of neutrino masses and mixing if NSI at source and/or detector are active. In the case of reactor experiments, this effect [?] has been studied in [18, 35, 36, 58], as well as in long baseline experiments [59, 60] where NSI matter effects could also be important. Because there are relatively model independent bounds from nuclear and particle decay and from very short-baseline experiments, there are bounds on source and detector NSI of ≤ 0.05 on most of the parameters [56]. These are independent of oscillation phenomena, which strongly limits the range of possible NSI induced error in determining the values of the neutrino mass and mixing parameters.

There is generally expected to be ambiguity and apparent tension among measurement of the basic neutrino mass and mixing parameters, possibly owing to NSI parameters. Global fits that involve both parameter sets are certainly warranted at each stage of advance in experimental scope and and precision. Our aim here has been to bring out the potential for low-energy solar neutrino physics to play a useful part in these future analyses.

VIII. SUMMARY AND CONCLUSIONS

As emphasized in the Introduction, we have focused on the use of low-energy, pp , ${}^7\text{Be}$ and pep Borexino direct observation results, published between 2011 and 2014 [6–8], to explore possible effects due to NU and FC NSIs.

The primary motivation was the relative insensitivity of the survival probability P_{ee} to matter effects, in the LMA-MSW picture, with or without effects due to NSI in neutrino-matter forward elastic scattering. This feature, within reasonable approximations, permits the focus to be on the direct NSI effects entering at the fusion process in the sun and the modifications to ν -e interactions at the detector.

After introducing our formulation and basic notation in Sec. II, we outlined the model calculation of neutrino interaction rates in Borexino in Sec. III. Then in Sec. IV we set all NSI parameter values to zero to find the best-fit value and allowed 1σ and 90% C.L. ranges of $\sin^2(\theta_W)$, extending the determination of the weak angle to the sub MeV energy region. We found $\sin^2(\theta_W) = 0.224 \pm 0.016$, consistent with the \overline{MS} PDG value 0.23126(5) at the Z-boson mass, renormalization group running values from the 100 GeV to 10 MeV range, 0.23867 ± 0.00016 [55], 0.2381(6) [54], and with another recent low-energy study [20]. Our estimate in Sec. 7 of the improvement in uncertainty possible with 1% solar data shows that the predicted value running to low-energy from the value at the Z-pole can be tested at about 98% C.L., but may not be sufficient to make a decisive determination.

In Secs. V, VI and VII we then reported and discussed the results of our χ^2 analysis of the measured rates vs. the modeled rates, looking systematically at allowed parameter boundaries of single and joint parameter choices for source alone, detector alone and combined source and detector. The results showed consistency¹⁰ with other solar studies that focussed on matter effects [14], or on NU NSI at the detector alone [40], or on short-baseline reactor data with both NU and FC NSI effects at source and detector [18, 19].

In Sec. VII we studied the impact that an improvement of the uncertainty in experimental rates to the 1% level, as targeted in a number of proposals for new generation solar neutrino or dark-matter experiments, where the solar neutrino background is recognized as a serious problem for experiments hoping to increase dark-matter search sensitivities to new levels. As expected, we found order of magnitude increases in sensitivity in some one parameter at-a-time bounds, though the two-parameter space source vs. detector level of improvements are mixed, due to largely to the high degree of correlation among some of the parameters. This is evidence of systematic compensation among terms in the fit functions, which leads to limited growth of overall sensitivity. Developing tests that break these degeneracies goes beyond the goal of this work to take a first look at bounds on source NSI using the recent Borexino low-energy data and to revisit bounds on detector NSI and to make a survey of the correlations between the two.

We conclude that current pp , ${}^7\text{Be}$ and pep neutrino rate measurements help narrow the range of lepton flavor violating NSI in both semi-leptonic and leptonic NSI cases and that future 1% measurements will greatly improve the search for new physics effects. At the same time, we have identified some strong correlations among NSI parameters and ambiguities between oscillation and NSI effects that make bounding some of the parameters a challenge and an important goal for future work.

The low-energy end of the solar neutrino spectrum will continue to be of great interest for decades to come for reasons of straight neutrino physics, solar physics and dark-matter physics. Our study showed the complementarity of NSI source and detector low-energy solar data analysis to other NSI searches. We found indications of limitations in our straightforward χ^2 treatment in the case of the source - detector cross correlation studies, which brings out the need to explore more comprehensive analyses to take full advantage of future experimental precision data.

IX. APPENDIX

A. The pp neutrino flux

We show the normalized pp electron neutrino spectrum based on Table IV from Ref. [1] in Fig. 9. As we mentioned in Sec. III A, the NSI forward scattering effects on the pp spectrum are very small [46], and we do not include them here. The dots in Fig. 9 are the SSM points of the pp normalized spectrum, and the red line is the curve of the fit function, Eq. (20). We assume the total flux to be $\Phi_{pp} = 5.98 \times (1 \pm 0.006) \times 10^{10} \text{ cm}^{-2} \text{ s}^{-1}$, corresponding to the high-metallicity model used in Borexino's publication [6] to calculate their expected rate of 131 ± 2 . The flux as a function of energy is then

$$\phi(E_\nu)_{pp} = \Phi_{pp} \times d\lambda(E_\nu)/dE_\nu, \quad (19)$$

¹⁰ The consistency is in the sense that some bounds are stronger, some are weaker and some are essentially the same.

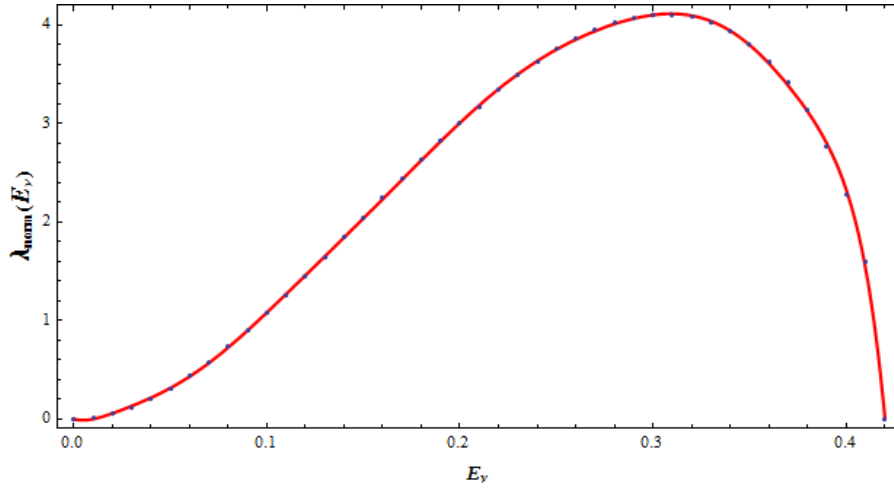


FIG. 9: Normalized pp spectrum $d\lambda/dE_\nu$ from Table IV of Ref. [1]

where the normalized flux energy distribution is fit by the power series,

$$\frac{d\lambda(E_\nu)}{dE_\nu}|_{fit} = \sum_{n=1}^{11} a_n (E_\nu)^{n-1}, \quad (20)$$

with the unit normalization maintained to one part in 10^4 . The fitting parameters are given in Table VII.

a_1	-6.21914	a_5	$-6.82779.10^6$	a_9	$-1.39822.10^9$
a_2	835.245	a_6	$5.06675.10^7$	a_{10}	$1.49676.10^9$
a_3	-28352.1	a_7	$-2.41275.10^8$	a_{11}	$-6.91255.10^{11}$
a_4	573193	a_8	$7.3743.10^8$	—	—

TABLE VII: The coefficients a_i for the fit to the data from Table IV of Ref. [1]

Acknowledgments

DWM thanks the Kavli Institute for Theoretical Physics at Santa Barbara, where this work was initiated during the Present and Future Neutrino Physics Workshop. ANK is thankful to O. Smirnov and Aldo Ianni of Borexino collaboration for the useful discussions and communication with them. The financial support to ANK for this work has been provided by the Sun Yat-Sen University under the Post-Doctoral Fellowship program.

-
- [1] Bahcall and Ulrich, "Solar models, neutrino experiments, and helioseismology", *Rev. Mod. Phys.* **60**, #2 (April 1988).
 - [2] R. Davis Jr., D. S. Harmer and K.C. Hoffman, *Phys. Rev. Lett.* **20**, 1205 (1968).
 - [3] M. Maltoni and A. Yu. Smirnov, "Solar neutrinos and neutrino physics", *Eur. Phys. J* **A52**, 87 (2016).
 - [4] A. Ianni, "Solar neutrinos and the solar model", *Physics of the Dark Universe* **4**, 44 (2014).
 - [5] W. C. Haxton, R. G. Robertson and A. Serenelli, "Solar Neutrinos: Status and Prospects", *Ann. Rev. Astron. Astrophys.* **51**, 21 (2013).
 - [6] G. Bellini *et al.* (Borexino Collaboration), "Neutrinos from the primary proton-proton fusion process in the Sun", *Nature* **512**, 383 (2014); arXiv:1308.0443v2 [hep-ex].
 - [7] G. Bellini *et al.* (Borexino Collaboration), "Precision Measurement of the ^7Be Solar Neutrino Interaction Rate in Borexino", *Phys. Rev. Lett.* **107**, 141302 (2011).

- [8] G. Bellini *et al.* (Borexino Collaboration), "First Evidence of *pep* Solar Neutrinos by Direct Detection in Borexino", *Phys. Rev. Lett.* **108**, 051302 (2012).
- [9] Recent reviews are: A. Derbin and V. Muratova *et al.* (Borexino Collaboration), "Main results of the Borexino Experiment", Proceedings of the Third Annual Large Hadron Collider Physics Conference, St. Petersburg, Russia (2015). arXiv:[1605.0679v1 [hep-ex], 22 May, 2016; O. Yu Smirnov *et al.*, "Measurement of Solar pp-neutrino flux with Borexino: results and implications", ICPPA-2015, Journal of Physics: Conference Series **675**, 012027 (2016).
- [10] S. P. Mikeyev and A. Yu. Smirnov, *Sov. J. Nucl. Phys.* **42**, 913 (1985).
- [11] L. Wolfenstein, "Neutrino oscillations in matter", *Phys. Rev. D* **17**, 2369 (1978).
- [12] P. C. Holanda and A. Yu. Smirnov, *J. Cosmol. Astropart. Phys.* **02**, 001 (2003).
- [13] A. Friedland, C. Lunardini and C. Peña-Garay, "Solar neutrinos as probes of neutrino-matter interactions", *Phys. Lett. B* **594**, 347 (2004).
- [14] M.C. Gonzalez-Garcia and M. Maltoni, "Determination of matter potential from global analysis of oscillation data", *JHEP* **1309**, 152 (2013).
- [15] R. Bonventre, A. LaTorre, J.R. Klein, G. D. Orebi Gann, S. Seibert, and O Wasalski, "Nonstandard models, solar neutrinos, and large θ_{13} ", *Phys. Rev. D* **88**, 053010 (2013).
- [16] A. Bolaños, A. O.G. Miranda, A. Palazzo, M.A. Tórtola, and J.W.F. Valle, "Probing nonstandard neutrino-electron interactions with solar and reactor neutrinos", *Phys. Rev. D* **79**, 113012 (2009).
- [17] S. Bergmann, M. M. Guzzo, P. C. Holanda, P. I. Krastev and H. Nunokawa, "Status of the solution to the solar neutrino problem based on nonstandard neutrino interactions", *Phys. Rev. D* **62**, 073001 (2000).
- [18] A. N. Khan, D. W. McKay and F. Tahir, "Short baseline reactor $\bar{\nu} - e$ scattering experiments and non-standard neutrino interactions at source and detector", *Phys. Rev. D* **90**, 053008 (2014).
- [19] A. N. Khan, "Global analysis of the source and detector nonstandard interactions using the short baseline neutrino- and antineutrino- electron scattering data", *Phys. Rev. D* **93**, 093019(2016).
- [20] B. C. Canas, E. A. Garces, O. G. Miranda, M. Tortola and J. W. F. Valle, "The weak-mixing angle from low-energy neutrino measurements: a global update", *Phys. Lett. B* **761**, 450 (2016).
- [21] M. Deniz *et al.* (TEXONO Collaboration), "Measurement of $\bar{\nu}_e$ -electron scattering cross section with a CsI(Tl) scintillating crystal array at the Kuo-Sheng nuclear power reactor" *Phys. Rev. D* **81**, 072001 (2010).
- [22] A. Aguilar *et al.* LSND Collaboration), *Phys. Rev. D* **64**, 112007 (2001).
- [23] B. Armbruster *et al.* (KARMEN Collaboration), *Phys. Rev. D* **65**, 112001 (2002).
- [24] M. Deniz *et al.* (TEXONO Collaboration), *Phys. Rev. D* **82**, 033004 (2010).
- [25] D. G. Cerdeño, M. Fairbairn, Thomas Jubb, P. A.N. Machado, A. C. Vincent, and C. Bøehm, "Physics from solar neutrinos in dark-matter direct detection experiments", *JHEP* **1605**, 118 (2016).
- [26] J. Billard, E. Figueroa-Feliciano and L. Strigari, "Implication of neutrino backgrounds on the reach of next generation dark-matter direct detection experiments", *Phys. Rev. D* **89**, 023524 (2014).
- [27] J. Billard, E. Figueroa-Feliciano, and L. Strigari, "Solar neutrino physics with low-threshold dark-matter detectors", *Phys. Rev. D* **91**, 095023 (2015).
- [28] J.-W. Chen, H.-C. Chi, C.-P. Liu and C.-P. Wu, "Low- energy electronic recoil in Xenon detectors by solar neutrinos", arXiv:1610.04177 [hep-ex] (2016).
- [29] J. Beacom *et al.* (The CJPL Collaboration), "Letter of Intent: Jinping Neutrino Experiment", arXiv: 1602.01733 v4 [physics.ins-det] (2016).
- [30] K. Abe *et al.* (Hyper-Kamiokande Collaboration), "Letter of Intent: The Hyper-Kamiokande Experiment-Detector Design and Physics Potential", arXiv:1109.3262 v1 (2011).
- [31] F. An *et al.* JUNO Collaboration, "Neutrino Physics with JUNO", *J. Phys. G* **43**, 03040 (2016); arXiv:1507.05613 [physics.ins-det]
- [32] M. Wurm *et al.* (LENA Collaboration), "low-energy Neutrino Astronomy in LENA", *Physics Procedia* **61**, 376 (2015); doi:10.1016/j.phpro.2014.12.078.
- [33] E.A. Garces, O.G. Miranda, M.A. Tortola and J.W.F. Valle, "Low-energy-electron scattering as a standard model probe: The potential of LENA as case study", *Phys. Rev. D* **85**, 073006 (2012).
- [34] S. Andringa *et al.* (SNO+ Collaboration), "Current Status and Future Prospects of the SNO+ Experiment", *Advances in High Energy Physics* **2016**, 6194250 (2016); arXiv: 1508.05759 v3 [physics.ins-det].
- [35] A. N. Khan, D. W. McKay and F. Tahir, "Sensitivity of medium baseline reactor neutrino mass-hierarchy experiments to nonstandard interactions", *Phys. Rev. D* **88**, 113006 (2013).
- [36] T. Ohlsson, H. Zhang and S. Zhou, "Nonstandard interaction effects on neutrino parameters at medium-baseline reactor antineutrino experiments", *Phys. Lett. B* **728**, 148 (2014).
- [37] L. M. Johnson and D. W. McKay, "Fitting direct interaction pieces into neutrino puzzles", *Phys. Lett. B* **433**, 355 (1998).
- [38] L. M. Johnson and D. W. McKay, "Revising neutrino oscillation parameter space with direct flavor-changing interactions", *Phys. Rev. D* **61**, 113007 (2000).
- [39] S. Bergmann and Y. Grossman, "Can lepton flavor violating interactions explain the LSND effect? ", *Phys. Rev. D* **59**, 093005 (1999).
- [40] S. K. Agarwalla, F. Lombardi and T. Takeuchi, "Constraining Non-Standard Interactions of the Neutrino with Borexino", *JHEP* **1212**, 079 (2012).
- [41] K. Nakamura and S.T. Petcov, "NEUTRINO MASS, MIXING, AND OSCILLATIONS", in Patrignani et al., (Particle Data Group), *Chin. Phys. C* **40**, 100001(2016).
- [42] D. W. McKay and L. M. Johnson, "Probing Lepton Flavor Violation", Proceedings of PASCOS 99, Lake Tahoe, NV (1999),

edited by K. Cheung, J. Gunion and S. Mrenna (World Scientific, Singapore, 2000), pp 204-207.

- [43] M. C. Gonzalez-Garcia, Y. Grossman, A. Gusso and Y. Nir, "New CP violation in neutrino oscillations", *Phys Rev. D* **64**, 096006 (2001).
- [44] J. N. Bahcall, M. Kamionkowski and A. Sirlin, "Solar neutrinos: Radiative corrections in neutrino-electron scattering experiments", *Phys. Rev. D* **51**, 6146 (1995).
- [45] A. M. Serenelli, W. C. Haxton and C. Peña-Garay, "Solar models with accretion -1. Application to the solar abundance problem." *Astrophys. J.* **743**, 24 (2011).
- [46] I. Lopes, "New neutrino physics and the altered shapes of solar neutrino spectra", *Phys. Rev. D* **95**, 015023 (2017).
- [47] V. Barger, R.J.N. Phillips and K. Whisnant, "Level crossings in solar-neutrino oscillations", *Phys. Rev. D* **34**, 980 (1986).
- [48] S.J. Parke, *Phys. Rev. Lett.* **57**, 1275 (1986).
- [49] V. Barger, D. Marfatia and K. Whisnant, "Testing the LMA solution with solar neutrinos independently of solar models", *Phys. Lett. B* **617**, 78 (2005).
- [50] I. Lopes and S. Turck-Chieze, "Solar neutrino physics oscillations: sensitivity to the electronic density in the Sun's core.", *Astrophys. J.* **765**, 14 (2013).
- [51] S. K. Agarwalla and Patrick Huber, "Potential measurement of the weak-mixing angle with neutrino-electron scattering at low-energy", *JHEP* **1108**, 059 (2011).
- [52] C. Bouchiat and S.A. Piketty, "Parity violation in atomic cesium and alternatives to the standard model of electroweak interactions", *Phys. Lett. B*, 128, 73 (1983).
- [53] C. S. Wood et al., "Measurement of Parity Nonconservation and an Anapole Moment in Cesium", *Science* **275**, 1759 (1997).
- [54] S. G. Porsev, K. Beloy and A. Derevianko, "Precision Determination of Electroweak Coupling from Atomic Parity Violation and Implications for Particle Physics", *Phys. Rev. Lett.* **102**, 181601 (2009).
- [55] J. Erler and M. J. Ramsey-Musolf, "weak-mixing angle at low energies", *Phys. Rev. D* **72**, 073003 (2005).
- [56] C. Biggio, M. Blennow, and E. Fernandez-Martinez, "Model independent bounds on nonstandard interactions ", *JHEP* **0908**, 090 (2009).
- [57] O.G. Miranda and H. Nunokawa, "Non-standard neutrino interactions: current status and future prospects", *New J. Phys.* **17**, 095002 (2015).
- [58] T. Ohlsson and H. Zhang, "Non-standard interaction effects in reactor neutrino experiments", *Phys. Lett. B* **671**, 99 (2009).
- [59] M. Blennow, S. Choubey, T. Ohlsson, D. Pramanik, S. K. Raut, "A combined study of source, detector and matter non-standard neutrino interactions at DUNE", *JHEP* **1608**, 090 (2016).
- [60] Pouya Bakhti, Amir N. Khan, "Sensitivities to charged-current nonstandard neutrino interactions at DUNE", arXiv:1607.00065